

Mechanical Properties of $\text{Hf}_x\text{NbTaTiZr}$ Refractory High-Entropy Alloys via Molecular Dynamics

Yankai Yu^{1,*}

¹School of Physics and Optoelectronic Engineering, Guangdong University of Technology, Guangzhou 510006, China

* Corresponding author

Abstract: Refractory high-entropy alloys (RHEAs) combine outstanding high-temperature strength with broad compositional tunability, yet they suffer from limited ductility at room temperature and decreased thermal stability. In this study, we use molecular-dynamic simulations to probe $\text{Hf}_x\text{NbTaTiZr}$ ($x = 0, 0.25, 0.50, 0.75, 1.00, 1.25, 1.50, 1.75, 2.00$) over 77-900 K. Uniaxial tension and nanoindentation reveal that raising Hf content expands the lattice ($3.382 \rightarrow 3.468 \text{ \AA}$) and, at 900 K, cuts the Young's modulus from 154.5 to 88.2 GPa and ultimate strength from 1,000 to 450 MPa while hardness drops by up to 47 %; intermediate Hf levels ($x = 0.50\sim 1.25$) retain low-temperature hardness. We identify the atomic-scale mechanisms—solid-solution weakening under thermal activation and phase-structure evolution—that govern these trends. These insights pave the way for designing RHEAs with an optimal balance of strength, ductility, and high-temperature stability for extreme-service applications.

Keywords: Refractory high-entropy alloys; Mechanical properties; Molecular dynamics.

1. Introduction

Conventional alloy systems usually follow the concept of a single principal element design, that is, using a certain metal element (such as Fe, Ni) as the matrix and achieving solid solution strengthening or precipitation strengthening by adding trace amounts of other elements (usually <5 at %). However, with the increasing requirements of modern engineering technology for the comprehensive performance of materials, the single performance optimization mode of

traditional alloys has become difficult to meet the demands of multi-field coupling service environments. In 2004, Professor Ye Junwei's team^[1,2]The classical definition of a high-entropy alloy requires that the atomic fraction of each main element be between 5% and 35%, and the mixed entropy be greater than $1.36R$ (R is the universal gas constant, $R=8.314 \text{ J/(mol}\cdot\text{K)}$) to maintain the stability^[3]Recent studies have shown that the mixed entropy of some quaternary and even ternary alloy systems can also break through the traditional alloy boundaries^[4,5]

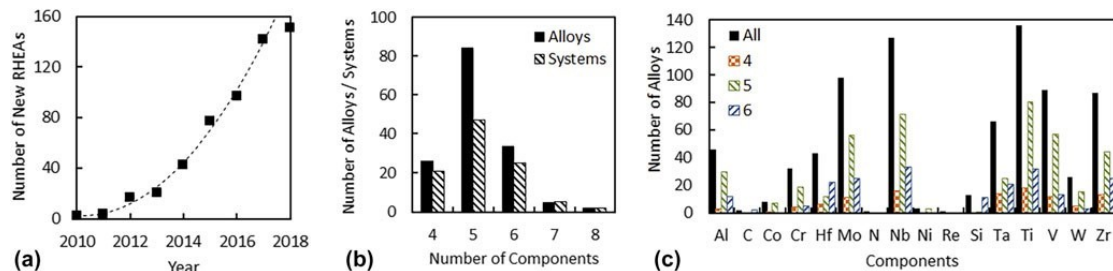


Figure 1. (a) Cumulative number of new RHEAs reported in the open literature as a function of the publication year, up to the end of January 2018. (b) Distribution of RHEAs and the alloy systems by the number of alloying elements. (c) Distribution of alloying elements in all reported RHEAs, as well as in 4-, 5-, and 6-component RHEAs^[6]

Based on the study of high-entropy alloys, Senkov et^[7] Typical refractory high-entropy alloys (such as WNbMoTaV) exhibit extraordinary hardness ($H_V > 4000 \text{ MPa}$) due to the strong covalent bond characteristics dominated by the BCC structure, which is significantly superior to traditional Ni-based superalloys. As shown in the statistics of Fig. 1(a), the refractory high-entropy alloy system has seen explosive growth since its proposal, with reported compositions ranging from quaternary to octic systems (see Fig. 1(c)), fully demonstrating the scalability of its composition space. At the microstructure level, refractory high-entropy alloys generally form BCC solid solutions with high dislocation density. Through the synergistic effect of multiple mechanisms such as lattice distortion strengthening and second-phase

precipitation strengthening, they show significant advantages in key indicators such as high-temperature strength ($>1200 \text{ }^\circ\text{C}$) and creep resistance, making them key candidate systems for hot-end component materials in extreme service environments.

2. Theoretical Basis and Research Methods

By using the MC+MD method, 1000 models were established for each system, from which the most stable model was selected, with a size of $20a \times 40a \times 20a$ (where a is the lattice constant) and a total of 32000 atoms. The time step was set to 0.001 ps. During the relaxation phase, set the boundary conditions to p p p and heat 100 ps from 1 K to the

set temperature (77 K, 300 K, 500 K, 700 K, 900 K) in the NPT ensemble. Then hold at 100 ps under the NPT ensemble for full relaxation. In the stretching simulation, the model boundary condition was set to p p p, and the relaxed model was subjected to uniaxial (Y) stretching simulation at a rate of $2.5 \times 10^8 \text{ s}^{-1}$ under the NPT ensemble. In the nanoindentation simulation, the model boundary condition was set to ppf, the Z-axis range of the model (0, 10 Å) was fixed, the virtual indentation ball radius was 18 Å, the indentation rate was 0.2 Å /ps for indentation into the model, and the virtual indentation ball was unloaded at the same rate when the indentation depth reached 12 Å until it left the model. The advantage of using a virtual indenter ball in the nanoindentation process is that it can reduce the complex interaction between the model atoms and the indenter, and there is no need to consider the force field between the model atoms and the indenter atoms, which greatly improves the feasibility and efficiency of nanoindentation simulation for multi-element models.

3. Mechanical Properties of $\text{Hf}_x\text{NbTaTiZr}$ Refractory Alloy

3.1. Model of $\text{Hf}_x\text{NbTaTiZr}$

To gain a deeper understanding of the properties of $\text{Hf}_x\text{NbTaTiZr}$ alloy, this study combined Monte Carlo and molecular dynamics methods to construct a series of component-controlled models. The system included different Hf component contents such as NbTaTiZr, $\text{Hf}_{0.25}\text{NbTaTiZr}$, $\text{Hf}_{0.50}\text{NbTaTiZr}$, $\text{Hf}_{0.75}\text{NbTaTiZr}$, $\text{Hf}_{1.00}\text{NbTaTiZr}$,

$\text{Hf}_{1.25}\text{NbTaTiZr}$, $\text{Hf}_{1.50}\text{NbTaTiZr}$, $\text{Hf}_{1.75}\text{NbTaTiZr}$ and $\text{Hf}_{2.00}\text{NbTaTiZr}$. Each model contains 32,000 atoms and relaxation simulations are conducted using NPT ensemble at different temperatures (77 K, 300 K, 700 K, 1100 K, 1500 K). Fig. 2 shows the atomic structure model of the $\text{Hf}_x\text{NbTaTiZr}$ alloy, as well as the atomic type distribution and radial distribution function (RDF) results of the HfNbTaTiZr alloy with the same molar ratio at different temperatures.

As shown in Fig. 2, with the increase of temperature, some atomic phase structure types undergo phase transformation within the $\text{Hf}_x\text{NbTaTiZr}$ alloy, changing from the original BCC phase to other phase structures. The relaxed RDF curves have distinct characteristics: the first main peak reflects the bonding strength between the nearest neighbor atoms, while the splitting phenomenon of the second main peak indicates that the system maintains the crystalline state characteristics. Therefore, it can be judged that the HfNbTaTiZr alloy system retains its crystal structure as a whole after relaxation at different temperatures. The increase in temperature enhances the thermal motion of atoms and weakens the interatomic interactions, resulting in a decrease in RDF peaks. In addition, the multi-peak structure in the RDF curve indicates a complex microstructure within the high-entropy alloy, which may involve multiple atomic arrangements and the presence of local order. Similar to the HfNbTaTiZr alloy with the same molar ratio, other alloy systems with Hf content also exhibit local phase transitions during the heating process and are in a crystalline state at all temperatures, which will not be elaborated further here.

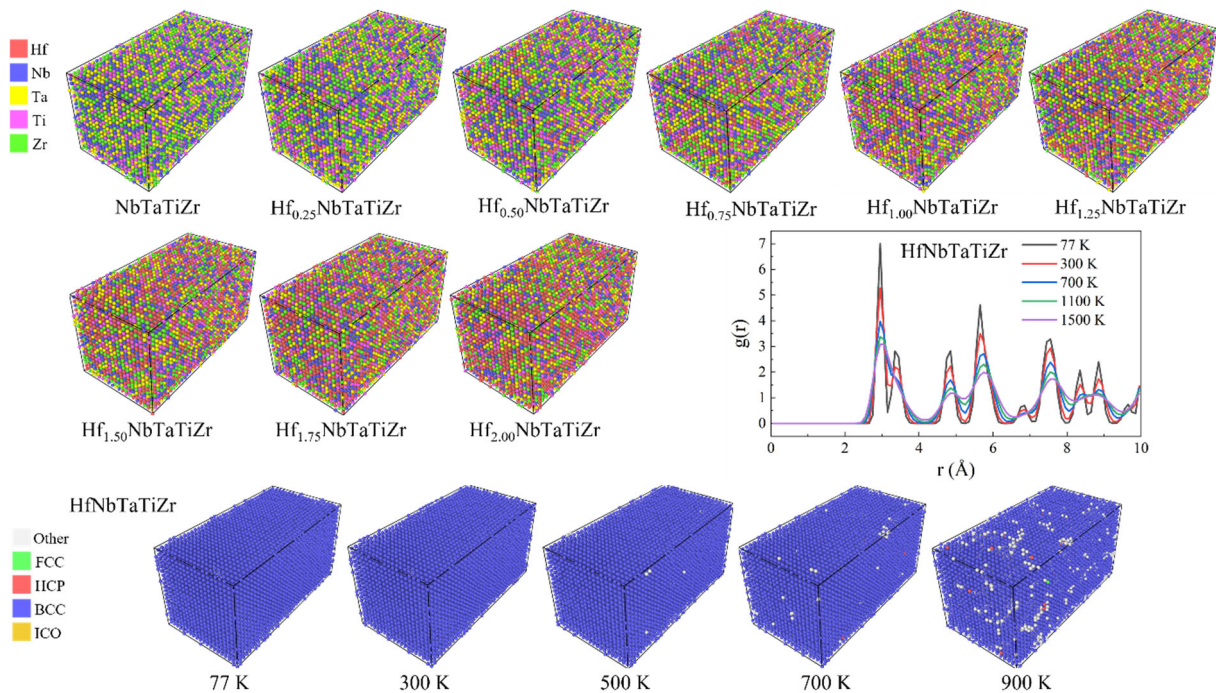


Figure 2. $\text{Hf}_x\text{NbTaTiZr}$ ($x = 0, 0.25, 0.50, 0.75, 1.00, 1.25, 1.50, 1.75, 2.00$) model at 300 K and the phase structure model and radial distribution function $g(r)$ of HfNbTaTiZr at different temperatures

3.2. Lattice constants of $\text{Hf}_x\text{NbTaTiZr}$

To understand the stability of BCC $\text{Hf}_x\text{NbTaTiZr}$ ($x = 0, 0.25, 0.50, 0.75, 1.00, 1.25, 1.50, 1.75, 2.00$) alloys with a single solid solution phase during heating, this study first simulated the structural relaxation of each component model at different temperatures. The lattice constant, a key

parameter, was extracted, and the results are shown in Table 1. The changing trend of the lattice constant can reflect the evolution process of the internal crystal structure of the alloy under thermal excitation, while the magnitude of the rate of change of the lattice constant during this heating process reveals the material's response ability to volume changes in

the thermal environment, which is of great reference value for evaluating its structural stability in high-temperature engineering applications.

It is notable that the lattice constants obtained from the $\text{Hf}_x\text{NbTaTiZr}$ alloy and the HfNbTaTiZr alloy model with the same molar ratio are close to the existing experimental results, and this comparison verifies the rationality of the established simulation model and the reliability of the simulation method. It can be clearly observed from the data in the table that the lattice constant of the $\text{Hf}_x\text{NbTaTiZr}$ refractory high-entropy

alloy shows a gradually increasing trend with the gradual increase of the Hf component content. The possible cause of this phenomenon lies in the atomic volume differences among the constituent elements of the alloy. The atomic volumes of Hf, Nb, Ta, Ti and Zr were $13.6 \text{ cm}^3/\text{mol}$, $10.87 \text{ cm}^3/\text{mol}$, $10.9 \text{ cm}^3/\text{mol}$, $10.64 \text{ cm}^3/\text{mol}$ and $14.1 \text{ cm}^3/\text{mol}$ respectively, with Hf having a larger atomic volume. When the content of the Hf component increased, the average distance between atoms in the lattice increased due to its larger atomic size, which led to an increase in the lattice constant.

Table 1. Lattice constant a of $\text{Hf}_x\text{NbTaTiZr}$ alloy at different temperatures

| Alloy | $a(\text{Å})$ 77 K | $a(\text{Å})$ 300 K | $a(\text{Å})$ 500 K | $a(\text{Å})$ 700 K | $a(\text{Å})$ 900 K |
|-----------------------------------|-----------------------|---------------------------|------------------------|------------------------|------------------------|
| NbTaTiZr | 3.382 | 3.387, 3.368 ^a | 3.392 | 3.398 | 3.406 |
| $\text{Hf}_{0.25}\text{NbTaTiZr}$ | 3.393 | 3.397 | 3.403 | 3.409 | 3.417 |
| $\text{Hf}_{0.50}\text{NbTaTiZr}$ | 3.402 | 3.407 | 3.411 | 3.419 | 3.426 |
| $\text{Hf}_{0.75}\text{NbTaTiZr}$ | 3.411 | 3.416 | 3.421 | 3.426 | 3.435 |
| $\text{Hf}_{1.00}\text{NbTaTiZr}$ | 3.418 | 3.423, 3.404 ^b | 3.428 | 3.435 | 3.442 |
| $\text{Hf}_{1.25}\text{NbTaTiZr}$ | 3.425 | 3.430 | 3.435 | 3.443 | 3.450 |
| $\text{Hf}_{1.50}\text{NbTaTiZr}$ | 3.431 | 3.436 | 3.441 | 3.448 | 3.457 |
| $\text{Hf}_{1.75}\text{NbTaTiZr}$ | 3.437 | 3.442 | 3.447 | 3.454 | 3.462 |
| $\text{Hf}_{2.00}\text{NbTaTiZr}$ | 3.442 | 3.447 | 3.453 | 3.460 | 3.468 |

^aReference^[8]

^bReference^[9]

In addition, $\text{Hf}_x\text{NbTaTiZr}$ alloys with different Hf component contents also showed a certain trend in the rate of change of the lattice constant with temperature (77~900 K). Specifically, NbTaTiZr (0.710%), $\text{Hf}_{0.25}\text{NbTaTiZr}$ (0.707%), $\text{Hf}_{0.50}\text{NbTaTiZr}$ (0.705%), $\text{Hf}_{0.75}\text{NbTaTiZr}$ (0.704%), $\text{Hf}_{1.00}\text{NbTaTiZr}$ (0.702%), $\text{Hf}_{1.25}\text{NbTaTiZr}$ (0.730%), $\text{Hf}_{1.50}\text{NbTaTiZr}$ (0.758%), $\text{Hf}_{1.75}\text{NbTaTiZr}$ (0.727%), $\text{Hf}_{2.00}\text{NbTaTiZr}$ (0.755%). This phenomenon indicates that an appropriate Hf component content has a positive effect on the thermal stability of $\text{Hf}_x\text{NbTaTiZr}$. When the temperature rises, the lower rate of change of the lattice constant means that the material has a stronger resistance to thermal strain at high temperatures, which helps to mitigate the internal stress and deformation caused by the temperature gradient, which has positive implications for the stability and service life of high-temperature structural materials. This discovery not only reveals the important role of Hf in regulating the thermal properties of refractory high-entropy alloys, but also provides theoretical support and design ideas for the development of high-temperature structural materials with excellent stability at high temperatures in the future.

3.3. Mechanical properties of $\text{Hf}_x\text{NbTaTiZr}$

Adjusting the composition content of Hf atoms to determine the most appropriate composition ratio is considered to effectively improve the mechanical properties of HfNbTaTiZr refractory high-entropy alloy. To explore the influence of Hf component content and its optimal ratio, this study systematically constructed $\text{Hf}_x\text{NbTaTiZr}$ ($x = 0, 0.25, 0.50, 0.75, 1.00, 1.25, 1.50, 1.75, 2.00$) models with different Hf component contents. Uniaxial stretching, nanoindentation and friction simulations were carried out, respectively. Through these multi-dimensional simulations, the effects and

evolution patterns of Hf component concentration and temperature on the strength, hardness and friction properties of this type of alloy were comprehensively evaluated.

In the stretching simulation, the strengthening and toughening mechanism of $\text{Hf}_x\text{NbTaTiZr}$ alloy was further revealed by analyzing the phase transformation behavior during the stretching process, providing important theoretical support for understanding the nature of its deformation. In addition, the regulation effect of temperature variation on the mechanical properties of $\text{Hf}_x\text{NbTaTiZr}$ was investigated in this section, and the structural response and performance variation patterns of HfNbTaTiZr at different service temperatures were clarified. These research results provide a scientific basis and technical guidance for optimizing the content of Hf components and improving the overall performance of high-entropy alloys in high-temperature and complex environments.

3.3.1. Uniaxial stretching simulation of $\text{Hf}_x\text{NbTaTiZr}$

To further investigate the effect of Hf component content on the mechanical properties of $\text{Hf}_x\text{NbTaTiZr}$ refractory high-entropy alloy, systematic single (Y) axis stretching molecular dynamics simulations were first carried out in this study. By constructing $\text{Hf}_x\text{NbTaTiZr}$ alloys with different Hf content ($x = 0, 0.25, 0.50, 0.75, 1.00, 1.25, 1.50, 1.75, 2.00$), The tensile behavior of HfNbTaTiZr alloy was analyzed under different temperature conditions (77 K, 300 K, 500 K, 700 K, 900 K), aiming to reveal the intrinsic connection between the variation of Hf content and the mechanical properties of the alloy at both macroscopic mechanical response and microstructure evolution levels, in order to simulate its performance under actual service conditions. And to provide theoretical support for the design of high-temperature structural materials.

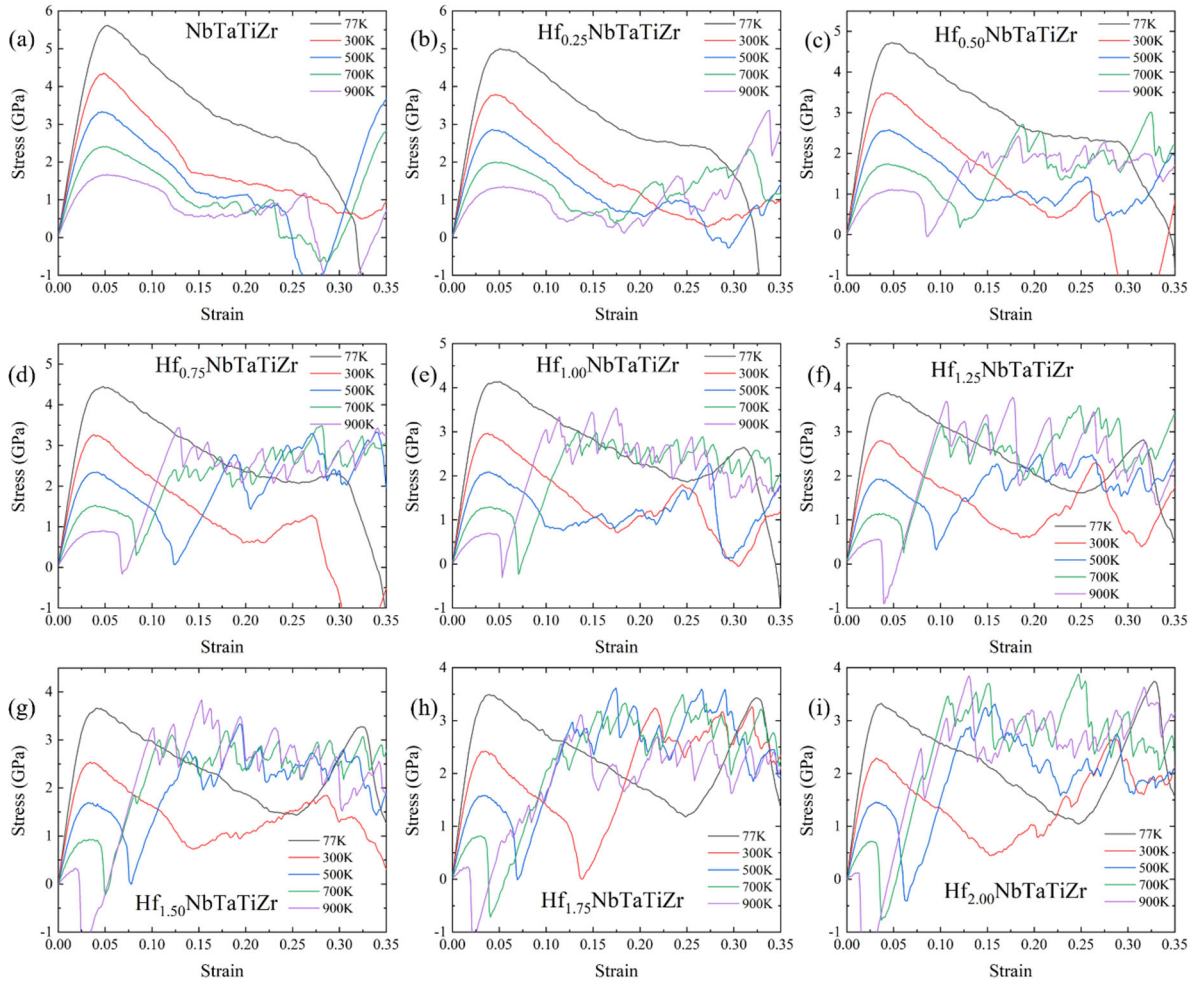


Figure 3. Uniaxial tensile simulation of $\text{Hf}_x\text{NbTaTiZr}$ ($x = 0, 0.25, 0.50, 0.75, 1.00, 1.25, 1.50, 1.75, 2.00$) at different temperatures

Fig. 3 shows the uniaxial tensile load-strain response curves of the $\text{Hf}_x\text{NbTaTiZr}$ series alloys at different temperatures. The typical stages that the high-entropy alloy undergoes during stretching can be clearly observed from the stress-strain curves: the elastic stage, the plastic deformation stage, and the strain hardening stage. In the early stage of elastic deformation, there is a linear relationship between the stress and strain of the alloy, following Hooke's law, indicating that the material has a good ability to reversibly deform during this stage. This stage is an important basis for evaluating the stiffness of the material against deformation. By selecting the low strain region of the curve (in this study, the strain range is $0 \sim 0.0056$) for linear fitting, the Young's modulus of the material can be extracted, which provides key mechanical parameters for subsequent analysis. As loading continues, the material gradually enters the plastic phase, which is characterized by a nonlinear increase in stress with strain, indicating the beginning of irreversible plastic deformation mechanisms such as slip, dislocation movement, and local structural rearrangement within the material. When the maximum stress value of plastic deformation is reached in the tensile curve, the material reaches its ultimate strength limit, and the strain value corresponding to the ultimate strength is the yield strain, a parameter that reflects the plasticity and ductility of the material during the tensile process, after which the stress value drops significantly. When the strain increases to a certain extent during the stress reduction process, the stress fluctuates greatly, a phenomenon known as strain hardening. The occurrence of strain

hardening can increase the strength of the material to a certain extent. The higher the temperature, the faster strain hardening occurs. For example, $\text{Hf}_{1.00}\text{NbTaTiZr}$ shows strain hardening at 77 K, 300 K, 500 K, 700 K and 900 K as 0.251, 0.176, 0.118, 0.071 and 0.053 respectively.

The role of Hf in regulating the stiffness, strength and plasticity of alloys can be explored by comparing the tensile responses of samples with different Hf content at different temperatures. Further combined with the analysis of the influence of temperature factors, it will help to fully understand the changes in the mechanical behavior of this refractory high-entropy alloy under extreme service conditions, thereby providing a theoretical basis for optimizing its high-temperature mechanical properties and structural stability.

Young's modulus, ultimate strength and yield strength are three important indicators in the evaluation of material mechanical properties. Among them, Young's modulus and ultimate strength are mainly used to measure the rigidity and load-bearing capacity of the material, that is, to reflect its ability to resist elastic deformation and tensile failure; Yield strain, on the other hand, is more focused on the stress limit that describes the elastic deformation of a material under external force. In order to systematically analyze the effect of Hf component content on the mechanical properties of $\text{Hf}_x\text{NbTaTiZr}$ refractory high-entropy alloy, this study first extracted Young's modulus and ultimate strength at Hf component content based on the tensile stress-strain curve using the previous method, and quantitatively statistically

analyzed and compared their variation patterns with Hf component content. In order to more intuitively reveal the

regulatory effect of Hf content on the strength and properties of the alloy.

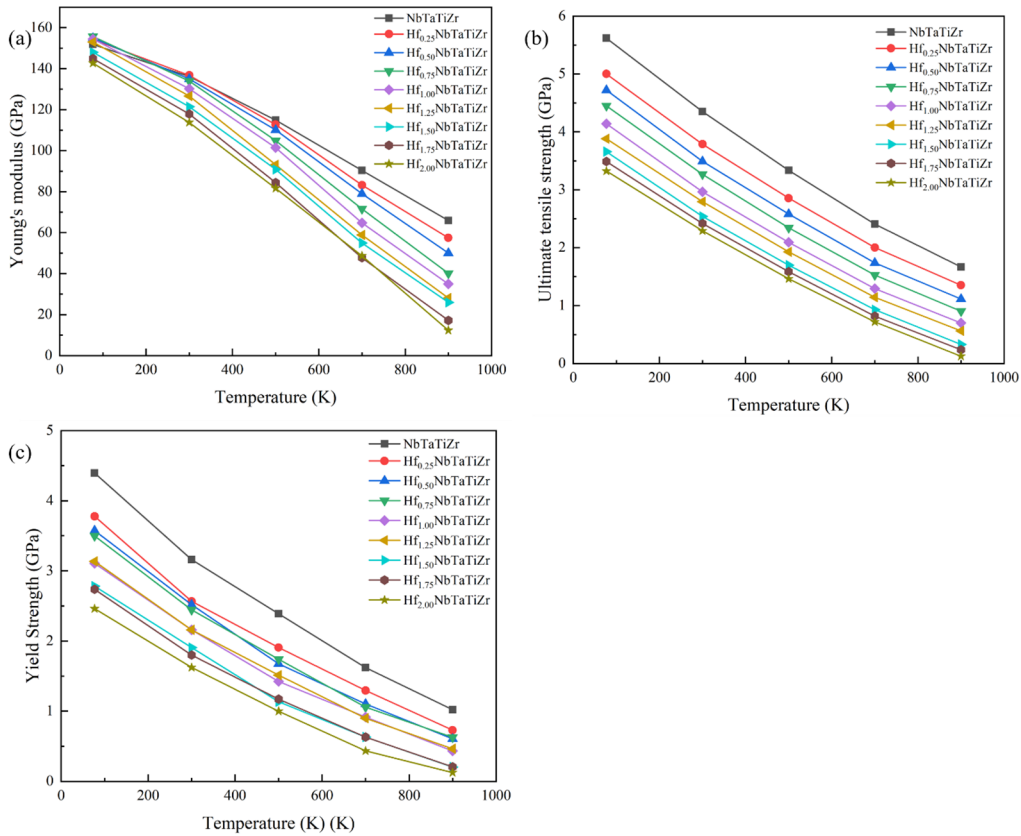


Figure 4. Changes in (a) Young's modulus, (b) ultimate strength and (c) yield strength of $Hf_xNbTaTiZr$ at different temperatures

Fig. 4 shows the trends of changes in Young's modulus, ultimate strength and yield strength of $Hf_xNbTaTiZr$ ($x = 0, 0.25, 0.50, 0.75, 1.00, 1.25, 1.50, 1.75, 2.00$) alloy at different temperatures. This reflects the key role that different concentrations of Hf atoms play in regulating the stiffness and strength of the alloy.

With the gradual increase in temperature, under the condition of the same Hf component content, the Young's modulus and ultimate tensile strength of $Hf_xNbTaTiZr$ alloy both show a significant decreasing trend, which indicates that the high-temperature environment will have a weakening effect on the overall strength properties of the material. As shown in Fig. 3, we can observe the changes in the stress-strain curve as the temperature increases. At high temperatures, the curve moves downward as a whole and the slope becomes smaller, which intuitively reflects the decrease in stiffness (Young's modulus) and maximum bearing capacity (ultimate tensile strength).

Further trend analysis reveals that the mechanical response of the alloy shows a consistent monotonically decreasing characteristic at different temperatures. Specifically, at room temperature (300 K), $Hf_{0.50}NbTaTiZr$ exhibited the highest Young's modulus (154.96 GPa) compared to quaternary NbTaTiZr (151.85 GPa) and equal molar ratio $HfNbTaTiZr$ (154.45 GPa), Higher by 3.11 GPa and 0.51 GPa, respectively; But in either system, as the temperature rose from room temperature to 900 K, the thermal activation effect intensified, resulting in a decrease in the interatomic interaction force, which led to significant drops in Young's modulus, ultimate tensile strength, and yield strength.

At the microscopic level, the increase in temperature first

intensifies the thermal vibration of the atoms, reduces the stability of the bonds between atoms, and promotes dislocation activity and the formation of local crystal defects. This causes strain hardening to occur earlier at higher temperatures: during stretching, the material undergoes local failure after reaching the ultimate tensile strength, but due to the rearrangement of internal dislocations and microscopic grain boundaries, secondary stress recovery occurs in some areas, resulting in the "inflection point" phenomenon on the stress-strain curve. This process can be visually seen in the illustration (e.g., the stress peak and recovery zone in Fig. 3), indicating that the internal deformation mechanism of the material at high temperatures is more complex than at low temperatures, with softening effects caused by thermal activation and strain hardening due to local reorganization.

Overall, in $Hf_xNbTaTiZr$ alloys at high temperatures, the increase in atomic thermal motion and dislocation activity due to temperature rise is the main cause of the reduction in overall stiffness, ultimate strength, and yield strength of the material; At the same time, the early emergence of strain hardening also reflects the local ordered changes in the microstructure and the transformation of the deformation mechanism. These phenomena not only provide intuitive support for the temperature dependence of the material's mechanical properties, but also offer a theoretical basis and engineering guidance for designing high-entropy alloys that are stable and durable for high-temperature applications.

3.3.2. Tensile microstructure analysis of $Hf_xNbTaTiZr$

In molecular dynamics studies in the field of high-entropy alloys, the optimization of alloy mechanical properties and phase transition mechanisms have always been the focus of

attention. Through uniaxial stretching simulations at room temperature, we found that the strengthening and toughening mechanisms of $\text{Hf}_x\text{NbTaTiZr}$ alloys are closely related to changes in their microstructure. Using Python to call the Ovito module for hierarchical statistics and analysis of the percentage of crystal structure categories and dislocation density in the sample helps to reveal the inherent laws of

crystal structure evolution during stretching and further explore the underlying mechanisms. Fig. 5 shows the trend of changes in the percentage of different crystal structures (such as BCC, FCC, HCP, and other disordered structures) during stretching, while Fig. 6 shows the curve of dislocation density varying with strain.

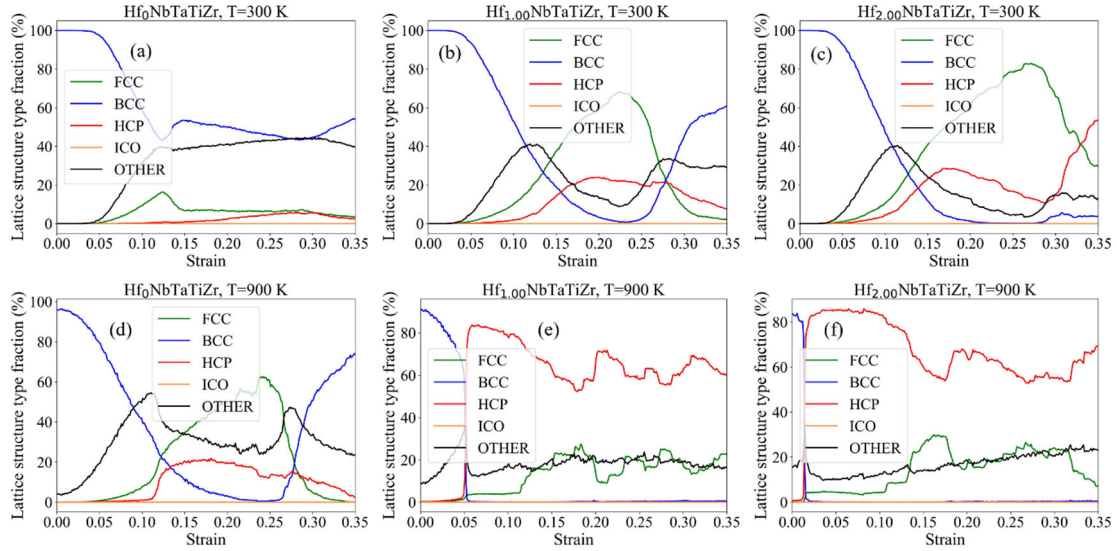


Figure 5. Percentage change of the crystal structure of some $\text{Hf}_x\text{NbTaTiZr}$ under 300 K and 900 K after tensile simulation

As can be seen from Fig. 5, in the early stage of stretching, the atoms in the sample mainly maintain the ordered BCC structure, at which time the internal crystal structure is relatively stable; As the strain increases, due to the higher surface energy of the surface atoms, some atoms start to transform from the BCC structure to other structures (mainly

FCC and HCP structures). As the stretching progresses, the proportion of BCC atoms drops sharply, replaced by a significant increase in FCC and HCP structures, a phenomenon that intuitively reflects the destructive effect of external stress on lattice equilibrium, resulting in a drastic reorganization of the internal crystal structure of the material.

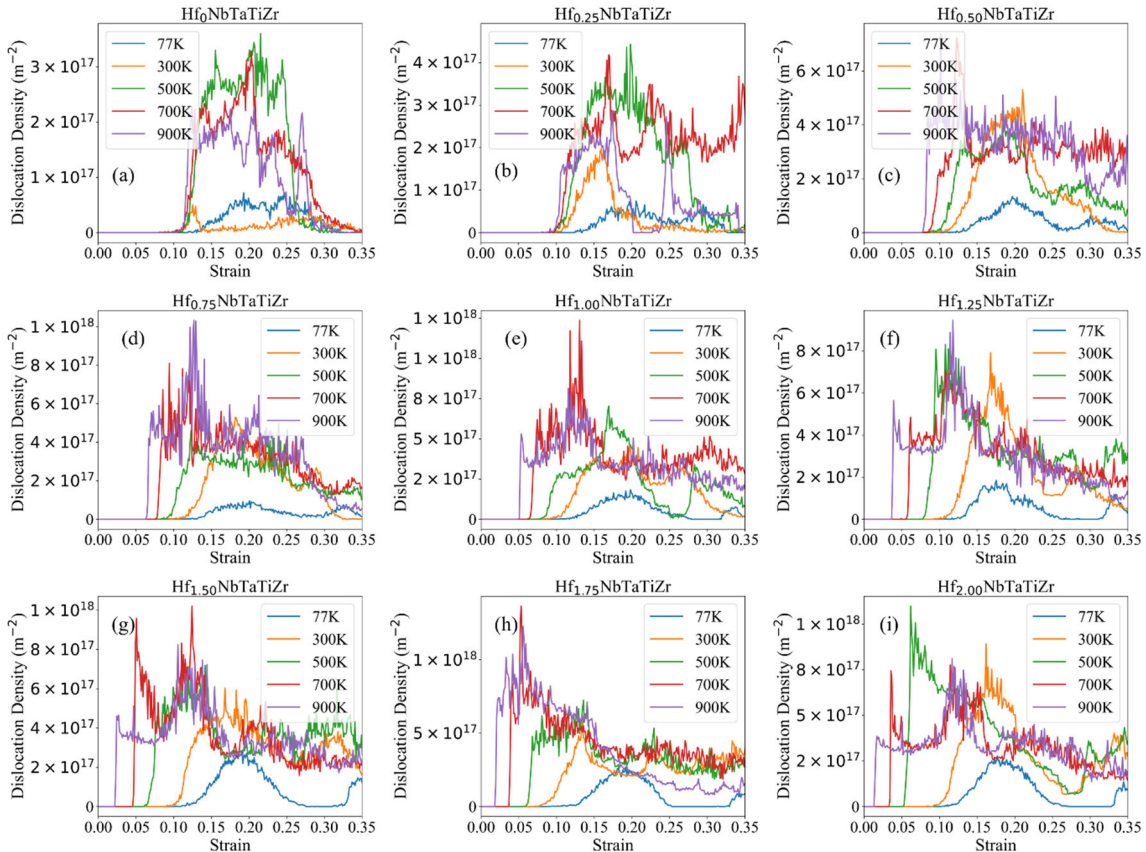


Figure 6. Dislocation density variation of $\text{Hf}_x\text{NbTaTiZr}$ in tensile simulation at 77 K ~ 900 K

Further trend analysis indicates that when the stress reaches the ultimate tensile strength, the ratio of FCC and HCP structure atoms exceeds that of the remaining BCC structure, suggesting a significant increase in plastic deformation of the material at this moment. Among them, the FCC structure, due to its larger number of slip planes, is more prone to dislocation slip under stress conditions, accelerating the plastic deformation process and causing the stress to drop rapidly; In contrast, the increase in the HCP structure leads to the formation of stacking faults, a defect that limits the further slip of dislocations, thereby causing strain hardening to a certain extent and enhancing the tensile stress in the local area.

At the microscopic mechanism level, the study shows that in the early stage of plastic deformation, the transformation from BCC to FCC structure is usually accompanied by a transition state similar to molten or amorphous intermediates, while the formation of HCP structure is mainly caused [10] Combining the proportion change of the crystal structure shown in Fig. 5 with the trend of rapid increase in dislocation density shown in Fig. 6, we can see that when the stress-strain

curve in Fig. 3 reaches the ultimate strength, the dislocation density suddenly rises, accompanied by the rapid formation of the FCC structure. The intense dislocation movement caused by the high dislocation density further promotes the formation of the HCP structure, while the accumulation of stacking faults hinders the further slip of dislocations, thereby making the strain hardening effect more pronounced, as shown by large fluctuations and undulations on the stress curve.

3.3.3. Nanoindentation simulation of $\text{Hf}_x\text{NbTaTiZr}$

Nanoindentation technology, as a commonly used mechanical property testing method, has unique advantages in evaluating the hardness, plastic behavior, and other mechanical properties of materials at the nanoscale. This study utilized nanoindentation simulations to conduct an in-depth investigation of $\text{Hf}_x\text{NbTaTiZr}$ refractory high-entropy alloys composed of different proportions of Hf at different temperatures, aiming to reveal the mechanism of performance evolution under extreme conditions.

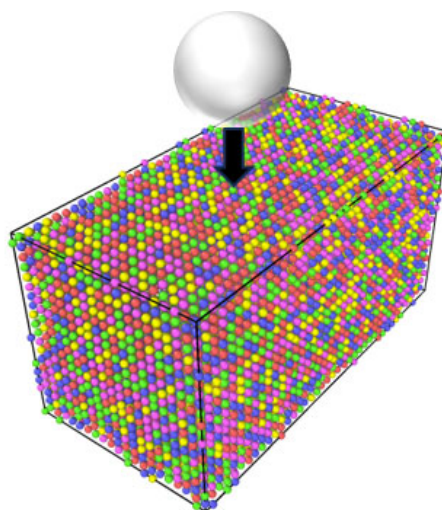


Figure 7. The MD models of nanoindentation on RHEAs, where the down pressing drill bit is a virtual nanosphere.

Boundary effects are a key factor that cannot be ignored when conducting nanoindentation tests, whether in experiments or molecular dynamics (MD) simulations. Especially in MD simulations, the boundary conditions used directly determine the extent to which the boundary effect affects.

In this study, we used periodic boundary conditions for the X and Y directions to effectively eliminate boundary effects on the side of the model. However, in the Z direction, due to the setting of non-periodic boundary conditions, the influence of the boundary effect was mainly reflected in the selection of indenter size and indentation depth. Typically, the depth of the plastic deformation area can reach 3.5 times the radius of the indenter. Therefore, to avoid the interference of the boundary effect, the radius of the indenter should be less than 1/3 of the model size in the Z direction, and the maximum indentation

depth should not exceed $2/3$ [11] In this study, a spherical indenter with a radius of 18 \AA and an indentation depth of 12 \AA was selected. Such a design can effectively eliminate the indenter size effect and boundary effect, thereby ensuring reliable mechanical response and mature plastic deformation behavior in the simulation process. In addition, studies have shown that variations in the size of the indenter can significantly affect the results of nanoindentation tests. In MD simulations of single-crystal aluminium, for example, as the indenter radius increases, the load and indentation depth required for dislocation nucleation also increase accordingly, and hardness values show a significant dimensional effect. [12] Therefore, the proper selection of the indenter size and indentation depth is crucial for obtaining accurate mechanical property parameters of the material.

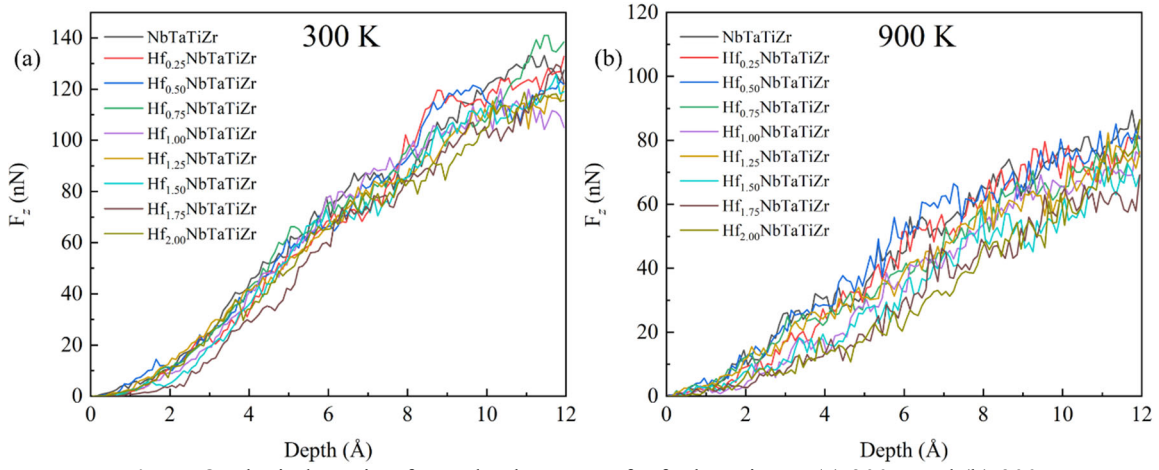


Figure 8. The indentation force-depth curves of $\text{Hf}_x\text{NbTaTiZr}$ at (a) 300K and (b) 900K

As shown in Fig. 8, the load-depth curves obtained from the nanoindentation simulation indicate that F_z is the load stress applied along the z direction. In the early stage when the indenter just begins to act on the material surface, the deformation is mainly concentrated on the surface layer of the material, causing the load stress to increase rapidly; As the indentation process continues, the material gradually enters the plastic deformation stage, and the increase in load stress slows down. In addition, at 900 K, there was a tendency for the load stress to decrease relatively. In order to more clearly analyze the effect of Hf content and temperature on indentation performance, contact area was used as a key parameter in this study, and the indentation hardness H of the material under nanoindentation was further calculated based on this parameter. The nanoindentation hardness of the high-entropy alloy can be given^[13] by the following formula:

$$H = \frac{P_{max}}{A_c} \quad (3.1)$$

Where P_{max} is the maximum stress of the load stress and A_c represents the projected area of the contact surface between the indenter and the alloy matrix in the Oxy plane.

$$A_c = \pi(2R - h)h \quad (3.2)$$

Where R is the radius of the spherical indenter and h is the depth of downpressing. In this study, P_{max} is the maximum value of F_z in Fig. 8, and h is the value of Depth corresponding to the maximum value of F_z .

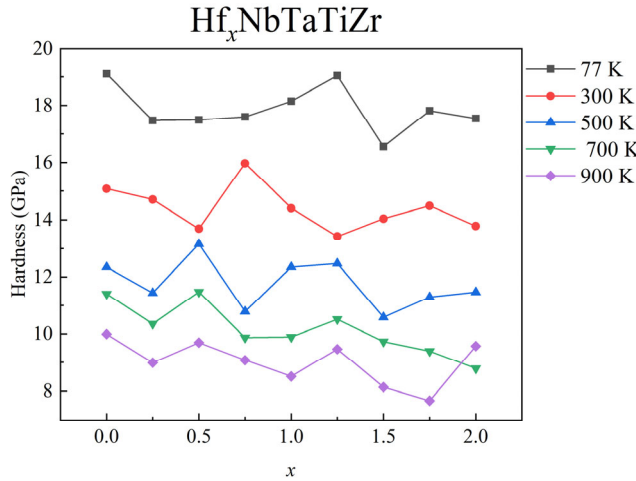


Figure 9. Changes in nanoindentation hardness of $\text{Hf}_x\text{NbTaTiZr}$ at different temperatures as a function of Hf component concentration

At high temperatures, most conventional metals typically experience a decrease in hardness, which is mainly attributed to dislocation activity and the thermal activation effect of crystal defects in the material. However, $\text{Hf}_x\text{NbTaTiZr}$ refractory high-entropy alloy, due to its well-regulated composition of elements, is expected to be able to design alloy systems that can maintain high hardness at high temperatures by adjusting the proportion of each component. As can be seen from Fig. 9, at the same temperature, with the increase of Hf component concentration, the change in

nanoindentation hardness does not show a simple monotony trend, but rather a complex nonlinear relationship. This reflects that when the Hf content changes the mechanical properties of the material, it not only affects the solid solution strengthening effect of the alloy, but may also cause changes in local crystal structure and dislocation behavior, thereby affecting the overall hardness of the material.

Specifically, the nanoindentation hardness data at various temperatures showed that NbTaTiZr had the highest hardness at 77 K, reaching 19.109 GPa; At 300 K, $\text{Hf}_{0.75}\text{NbTaTiZr}$ had

a hardness of 15.968 GPa; At 500 K and 700 K, Hf_{0.50}NbTaTiZr showed hardness of 13.161 GPa and 11.472 GPa, respectively; At 900 K, NbTaTiZr had a hardness of 9.987 GPa. These absolute hardness values reflect, to some extent, the strength performance of the alloy system at high temperatures. However, the effect of temperature variation on material properties in practical applications is more critical. Therefore, in this study, the rates of change in nanoindentation hardness for each Hf content system from room temperature (300 K) to high temperature (900 K) were further calculated as follows: NbTaTiZr (33.747%), Hf_{1.50}NbTaTiZr (38.883%), HfNbTaTiZr (29.244%), HfNbTaTiZr (43.174%), HfNbTaTiZr (40.929%), HfNbTaTiZr (29.53%), HfNbTaTiZr (42.033%), Hf_{2.00}NbTaTiZr (47.07%) and HfNbTaTiZr (30.564%).

These rates of change reflect the sensitivity of the material's hardness to temperature changes - the smaller the rate of change, the lower the material's dependence on temperature, and its hardness is relatively stable. In this study, it can be seen that the Hf_{1.75}NbTaTiZr system has the highest rate of hardness change (47.07%), indicating that this system is most sensitive to temperature changes; Hf_{0.50}NbTaTiZr (29.244%) and Hf_{1.25}NbTaTiZr (29.53%) showed less temperature sensitivity, with their hardness changing more gently as the temperature rose. This non-monotonic hardness change suggests that when regulating high-temperature performance, we should not only consider the value of absolute hardness, but also pay more attention to the comprehensive assessment of performance stability at temperature. By comparing the performance responses of different Hf component content systems under the same temperature gradient, valuable guidance and theoretical basis can be provided for designing high-entropy alloys with high hardness and thermal stability at high temperatures.

4. Conclusions

This work mainly conducted a systematic study on the mechanical properties of Hf_xNbTaTiZr refractory high-entropy alloys at different temperatures and with different Hf component contents through uniaxial stretching and nanoindentation simulations, and conducted multi-angle analyses from macroscopic mechanical responses to microstructure evolution, providing a theoretical basis for optimizing the performance of the alloy at high temperatures.

In the uniaxial stretching simulation section, alloy models with different Hf contents at $x = 0, 0.25, 0.50, 0.75, 1.00, 1.25, 1.50, 1.75,$ and 2.00 were constructed and their stress-strain responses were investigated at temperatures of 77 K, 300 K, 500 K, 700 K, and 900 K. The results showed that the alloy went through typical elastic, plastic and strain hardening phases during stretching. In the early stage, the material exhibits linear elastic properties, and Young's modulus can be extracted using linear fitting in the low strain range; As the strain increases, the material gradually enters the plastic deformation stage, showing nonlinear stress growth, and eventually obvious strain hardening occurs after reaching the ultimate strength. Temperature has a significant impact on all mechanical properties: as the temperature rises, the thermal activation effect intensifies, leading to increased atomic thermal vibration and dislocation activity, which in turn significantly reduces Young's modulus, ultimate strength, and yield strain; At the same time, strain hardening occurs earlier at high temperatures, indicating that the microstructure inside the material is undergoing drastic reconstruction, mainly

manifested as the crystal structure changing from the stable BCC to the FCC and HCP structures with more slip planes.

In nanoindentation simulations, a spherical indenter was used to locally load the alloy surface, and indentation load-depth curves and corresponding hardness data were obtained. The study further quantified the nanoindentation hardness of different Hf component systems at 300 K to 900 K and its rate of change with temperature by calculating the contact area. The results show that the hardness of the alloy does not simply change linearly with Hf doping, but rather exhibits complex non-monotonicity; Meanwhile, there are significant differences in the sensitivity of different systems to temperature changes, with some systems maintaining relatively stable hardness levels at high temperatures, which provides guidance for the design of alloy systems that have both high hardness and high-temperature stability.

Overall, through multi-scale mechanical simulations, we revealed the combined regulatory effect of Hf component content and temperature on the mechanical properties of Hf_xNbTaTiZr high-entropy alloy. The analysis of tensile and nanoindentation simulations not only reflects the changing trends of material strength and hardness at a macroscopic level, but also explains the basic physical processes of the material deformation mechanism at high temperatures through the analysis of microstructure and dislocation evolution. These results provide solid theoretical and technical support for further optimization design of alloy properties at high temperatures and for countering structural failure under extreme conditions.

Acknowledgment

This work was supported by the National Natural Science Foundation of China (Grant No. 11804057 and 12374069) and the Science and Technology Plan Project of Guangzhou, China (Grant No. 202102020655). We thank the Center of Campus Network & Modern Educational Technology, Guangdong University of Technology, Guangdong, China for providing computational resources and technical support for this work.

Declaration of interests

The authors declare that they have no known competing financial interests or personal relationships that could have appeared to influence the work reported in this paper.

The authors declare the following financial interests/personal relationships which may be considered as potential competing interests:

Minru Wen reports financial support was provided by National Natural Science Foundation of China. Minru Wen reports financial support was provided by Science and Technology Plan Project of Guangzhou, China. If there are other authors, they declare that they have no known competing financial interests or personal relationships that could have appeared to influence the work reported in this paper.

References

- [1] Yeh J W, Chen S K, Lin S J, et al. Nanostructured high entropy alloys with multiple principal elements: novel alloy design concepts and outcomes[J]. *Advanced engineering materials*, 2004, 6(5): 299-303.

- [2] Cantor B, Chang I T, Knight P, et al. Microstructural development in equiatomic multicomponent alloys[J]. *Materials Science and Engineering: A*, 2004, 375: 213-218.
- [3] Yong Zhang. *Advanced High Entropy Alloy Technology*[M]. Chemical Industry Press, 2019.
- [4] Senkov O, Senkova S, Miracle D, et al. Mechanical properties of low-density, refractory multi-principal element alloys of the Cr–Nb–Ti–V–Zr system[J]. *Materials Science and Engineering: A*, 2013, 565: 51-62.
- [5] Guo W, Dmowski W, Noh J-Y, et al. Local atomic structure of a high-entropy alloy: an X-ray and neutron scattering study[J]. *Metallurgical and Materials Transactions A*, 2013, 44: 1994-1997.
- [6] Senkov O N, Miracle D B, Chaput K J, et al. Development and exploration of refractory high entropy alloys—A review[J]. *Journal of materials research*, 2018, 33(19): 3092-3128.
- [7] Senkov O, Wilks G, Miracle D, et al. Refractory high-entropy alloys[J]. *Intermetallics*, 2010, 18(9): 1758-1765.
- [8] Nguyen V, Qian M, Shi Z, et al. A novel quaternary equiatomic Ti-Zr-Nb-Ta medium entropy alloy (MEA)[J]. *Intermetallics*, 2018, 101: 39-43.
- [9] Tseng K-K, Juan C-C, Tso S, et al. Effects of Mo, Nb, Ta, Ti, and Zr on mechanical properties of equiatomic Hf-Mo-Nb-Ta-Ti-Zr alloys[J]. *Entropy*, 2018, 21(1): 15.
- [10] Bordoloi P, Hazarika M P, Tripathi A, et al. Plasticity and strength of an equiatomic and a non-equiatomic HfNbTaTiZr high entropy alloy during uniaxial loading: A molecular dynamics simulation study[J]. *Materials Research Express*, 2024, 11(9): 096517.
- [11] Liu X, Hua D, Wang W, et al. Atomistic understanding of incipient plasticity in BCC refractory high entropy alloys[J]. *Journal of Alloys and Compounds*, 2022, 920: 166058.
- [12] Wugui Jiang, Junwan Li, Jianjun Su, et al. Quasi-continuum analysis of indenter size effect in nanoindentation test[J]. *Chinese Journal of Solid Mechanics*, 2007, 28(4): 375-379.
- [13] Guo Q, Hou H, Pan Y, et al. Hardening-softening of Al_{0.3}CoCrFeNi high-entropy alloy under nanoindentation[J]. *Materials & Design*, 2023, 231: 112050.